Actuators for the generation of highly nonlinear solitary waves

Xianglei Ni,[1] Piervincenzo Rizzo,[1,a)] and Chiara Daraio[2]
[1]*Department of Civil and Environmental Engineering, University of Pittsburgh, 942 Benedum Hall, 3700 O'Hara Street, Pittsburgh, Pennsylvania 15261, USA*
[2]*Applied Physics, California Institute of Technology, 1200 E California Boulevard, MC 105-50, Pasadena, California 91125, USA*

(Received 6 December 2010; accepted 29 January 2011; published online 10 March 2011)

In this paper we present the design of two actuators for the generation of highly nonlinear solitary waves (HNSWs), which are mechanical waves that can form and travel in highly nonlinear systems. These waves are characterized by a constant spatial wavelength and by a tunable propagation speed, dependent on the wave amplitude. To date, the simplest and widely adopted method to generate HNSWs is by impacting a striker onto a chain of beads of equal size and mass. This operation is conducted manually and it might be impracticable if repetition rates higher than 0.1 Hz are necessary. It is known that the HNSWs' properties, such as amplitude, duration, and speed can be modified by changing the size or the material of the particles, the velocity of the striker, and/or the precompression on the chain. To address the limitations associated with the manual generation of HNSWs we designed, built, and tested two actuators. The first actuator consists of a chain of particles wrapped by an electromagnet that induces static precompression on the chain. This design allows for the generation of solitary waves with controlled properties. The second actuator consists of a chain surmounted by an electromagnet that lifts and releases a striker. This actuator permits the remote and noncontact generation of solitary waves. The performance of both actuators is evaluated by comparing the experimental HNSWs to theoretical predictions, based on the long wavelength approximation. [doi:10.1063/1.3556442]

I. INTRODUCTION

Highly nonlinear solitary waves (HNSWs) are mechanical waves that can form and travel in highly nonlinear systems. One of these systems consists of a closely packed chain of elastically interacting particles (i.e., granular crystals).[1–25] The duration, amplitude, and speed of HNSWs can be tuned by adding static precompression on the system or varying the particles' material and geometry.[2,9,10,13] This tunability makes the use of HNSWs appealing in several engineering applications such as nondestructive testing[26–28] or acoustic imaging.[29]

The most common way to induce the formation and propagation of HNSWs in one-dimensional granular crystals is by impacting the first bead of the chain with a striker having the same mass of the particles composing the chain. The falling height of the striker determines the impact's speed which, in turn, affects the characteristics of the solitary pulse. The operation is conducted by manually lifting and then releasing the striker. To add precompression to a chain of spherical particles Coste *et al.*[4] applied a contact static force, which had the disadvantage of changing the boundary conditions. Daraio *et al.*[13] instead used a permanent circular magnet. This configuration removed any drawback associated with the boundary conditions but constrained the system to a single predefined static force.

In this paper we present the design of two actuators for the generation of HNSWs. The first actuator consists of a one-dimensional chain surrounded by an electromagnet. This configuration allows the creation of a controlled static precompression force spanning from 0 to 2 N that can be used to tune some of the solitary waves' properties. With respect to the solutions proposed in Refs. 4 and 13, the present actuator does not constrain the system to a single static compressive force.

The second actuator consists of a one-dimensional chain of particles surmounted by an electromagnet that lifts and releases the striker from a certain height. By remotely activating the electromagnet the movement of the striker can be guaranteed with a high level of repeatability. This noncontact excitation of HNSWs could be useful in applications where a remote placement of equipment or a complex geometrical arrangement of the chains is required. Moreover, the repetition rate at which a wave can be generated is higher, which makes the use of this actuator appealing in applications such as nondestructive testing[26] or acoustics.[29]

The actuators' ability to generate HNSWs was assessed by comparing the experimental results to the theoretical prediction obtained from the long-wave approximation.[2]

II. THEORY

For the sake of completeness a brief overview on the theory of HNSWs propagation is given here. For a more detailed formulation, interested readers are referred to Refs. 1–3,9, and 13.

In the continuum approximation (long-wavelength limit), the speed of the solitary wave V_s in a chain of beads subjected to an initial strain ξ_0 (or, in the discrete case, to a static force

a)Author to whom correspondence should be addressed. Electronic mail: pir3@pitt.edu. Tel.: (412) 624-9575.

F_0) is given as[2,13]

$$V_S = c_0 \frac{1}{(\xi_r - 1)} \left\{ \frac{4}{15}\left[3 + 2\xi_r^{5/2} - 5\xi_r\right] \right\}^{1/2}$$
$$= 0.9314 \left(\frac{4E^2 F_0}{a^2 \rho^3 (1-\nu^2)^2} \right)^{1/6} \frac{1}{\left(f_r^{2/3} - 1\right)}$$
$$\times \left\{ \frac{4}{15}\left[3 + 2f_r^{5/3} - 5f_r^{2/3}\right] \right\}^{1/2}, \quad (1)$$

where a is the diameter of the beads, and ρ, ν, and E are the density, Poisson's ratio and Young's modulus of the material, respectively. In Eq. (1), ξ_r is the maximum dynamic strain ξ_m normalized with respect to the static strain ξ_0:

$$\xi_r = \frac{\xi_m}{\xi_0}, \quad (2)$$

while the normalized force f_r is given by

$$f_r = \frac{F_m}{F_0}, \quad (3)$$

where F_m is the maximum force between the particles in the discrete chain.

The speed of a solitary wave in a "sonic vacuum"[13] is obtained when f_r is very large and it is expressed as

$$V_S = 0.6802 \left(\frac{2E}{a\rho^{3/2}(1-\nu^2)} \right)^{1/3} F_m^{1/6}. \quad (4)$$

The shape of a solitary wave with a speed V_S in a "sonic vacuum" can be closely approximated by[2]

$$\xi = \left(\frac{5V_S^2}{4c^2} \right) \cos^4 \left(\frac{\sqrt{10}}{5a} x \right), \quad (5)$$

where

$$c = \left(\frac{2E}{\pi\rho(1-\nu^2)} \right)^{1/2}. \quad (6)$$

The value of the dynamic contact force between two grains, F_m, can be computed by using the following relationship:

$$F_m = \beta F_{m,e} + F_0, \quad (7)$$

where $F_{m,e}$ is the force measured experimentally by a piezoelement embedded in one of the particles in the chain (as described in Ref. 9), and β is a coefficient associated with the particle's material and size. In this study we used the values of the coefficient β provided in Fig. 2 of Ref. 13.

III. ACTUATOR 1

The first actuator consisted of a polytetrafluoroethylene (PTFE) tube having inner diameter equal to 4.8 mm. The tube contained 20 low-carbon steel beads. The diameter of each sphere was equal to 4.76 mm and the mass was 0.45 g. Two 0.27 mm thick and 2 mm side piezogauges made from lead zirconate titanate were embedded inside two of the steel particles. The assembling and calibration of the instrumented particles were similar to that described in Refs. 2, 9 and 21. The

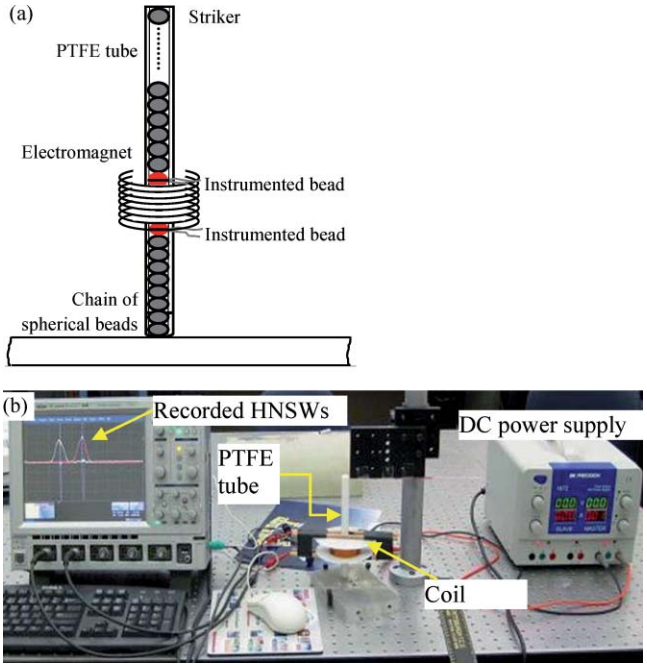

FIG. 1. (Color online) (a) Schematic diagram showing the chain of particles and the location of the coil. (b) Digital image of the setup.

beads with the embedded sensors were positioned along the chain at the 7th and 12th positions from the top and they were connected to an oscilloscope that sampled the signals at 10 MHz. To compare the experimental results with the theoretical predictions, the force $F_{m,e}$ measured by the instrumented bead was related to the dynamic contact forces (F_m) as described in Ref. 9 and by Eq. (7).

The portion of the chain of particles bounded by the piezosensors was enwound with a coil made of AWG24 magnetic wire. The coil consisted of about 1350 turns, was 23.8 mm long, which is five times the beads' diameter, and its electrical resistance was equal to 11.1 Ω. A dc power supply (BK Precision Model 1672) was used to provide electrical current to the coil. Because the electrical resistance of the coil depends on the coil temperature, the power supply was used in current control mode to keep the current constant. A schematic diagram and a photograph of the experimental setup are presented in Fig. 1.

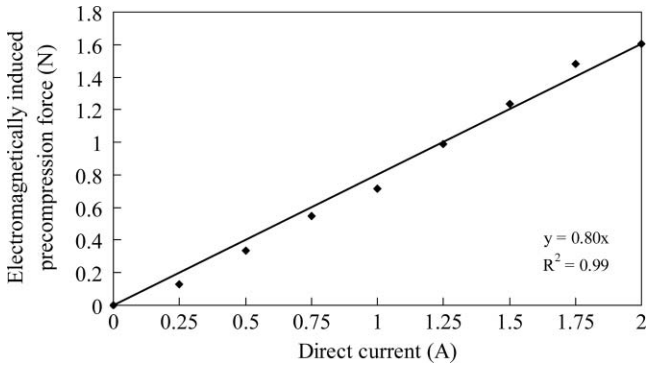

FIG. 2. Electromagnetically induced precompression force as a function of the electrical current provided by the dc power supply.

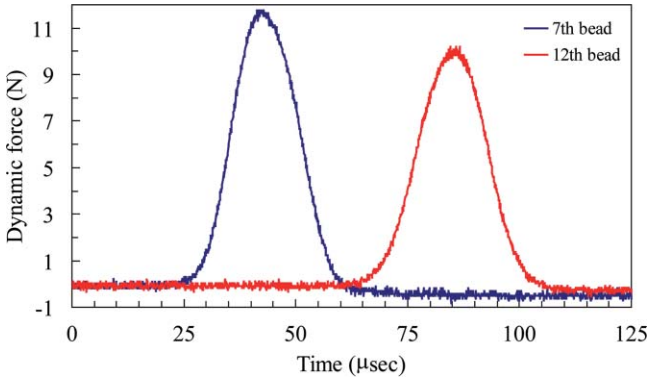

FIG. 3. (Color online) Typical HNSWs pulses observed by using actuator 1.

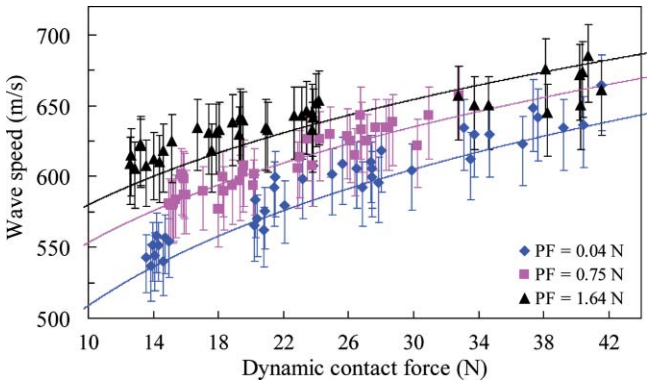

FIG. 4. (Color online) Wave speed as a function of the dynamic contact force at different amounts of static precompression force. The experimental values are shown by solid dots. The theoretical curves based on Eq. (1) for the different values of static precompression applied to the chain are represented by solid lines. The vertical error bars are the results of possible inaccuracy on the estimation of the peak's arrival time and on the measurement of the travel distance between the two piezosensors.

The relationship between the dc current and the force applied by the solenoid was empirically determined by measuring the weight that the electromagnet was able to lift. Figure 2 shows the force as a function of the current applied to the coil. It can be seen that the static force is linearly proportional to the current.

To evaluate the effectiveness of the actuator in tuning the properties of the propagating signals, the chain was impacted with a striker of equal shape and mass of the particles composing the chain falling from four different heights: 10, 20, 35, and 60 mm. For each impact, the static precompression was obtained by increasing the electrical current from 0 to 2 A at 0.25 A increments. For each combination of static force and striker's speed, ten measurements were taken to increase the statistical significance of the experiment and investigate the repeatability of the setup.

Figure 3 shows the time history of the force measured by both piezosensors when no current was allowed to pass through the coil. In this case, the static precompression was equal to 0.04 N (which corresponds to the gravitational preload of the particles as measured in the middle between the two piezosensors). The striker was released from 10 mm above the chain.

The speed of the solitary waves was determined by dividing the difference of the peaks' arrival time by the distance between the piezoelectric transducers. This distance was considered to be equal to five particles' diameters. We calculated the speed of propagation of the traveling waves at different levels of static precompression. Figure 4 illustrates the wave speed as a function of the dynamic contact force F_m for three precompression forces (PFs), namely, 0.04, 0.75, and 1.64 N. The values of 0.75 and 1.64 N were obtained by feeding the coil with 1 and 1.75 A, respectively. It should be noted that the design of the electromagnet was such that by using a current of 3 A, a static force equal to 2.3 N was attained. However, the excessive heat induced in the system prevented the usage of such high current for the time necessary to complete a round of measurements.

We took ten measurements for each level of PF and, to simulate various actuator configurations, the striker particle was dropped from four different heights: 10, 20, 35, and 60 mm, corresponding to four different impact velocities. The error bars shown in Fig. 4 refer to the uncertainty associated with the estimation of the peak's arrival time and the measurement of the travel distance between the two piezosensors. The experimental data are superimposed to the theoretical predictions obtained from Eq. (1). For each PF level, the data are largely clustered into four groups that correspond to the four falling heights of the striker. Higher striker velocities generate larger dynamic contact force in the system.

In order to quantify the error between the experimental data (the dots in Fig. 4) and the theoretical prediction (based on Eq. (1)), Table I lists the maximum and the average error that occurred within each set of ten measurements. For each experimental wave speed $V_{S,\mathrm{exp}}$, the error err(%) was computed as

$$\mathrm{err}(\%) = \frac{|V_{S,\mathrm{exp}} - V_{S,\mathrm{theor}}|}{V_{S,\mathrm{theor}}} \times 100, \tag{8}$$

where $V_{S,\mathrm{theor}}$ is calculated from Eq. (1). The overall agreement between the theoretical prediction and the empirical data is very good. This validates the design of the actuator, which

TABLE I. The maximum and average relative errors of wave speeds.

	Maximum error (%)			Average error (%)		
Height (mm)	$I = 0$ A	$I = 1$ A	$I = 2$ A	$I = 0$ A	$I = 1$ A	$I = 2$ A
10	3.80	2.96	4.48	2.02	0.95	2.76
20	4.56	2.90	3.76	2.12	0.91	2.53
35	3.33	1.91	2.52	1.64	0.90	1.43
60	4.24	2.86	4.35	1.87	1.46	1.94

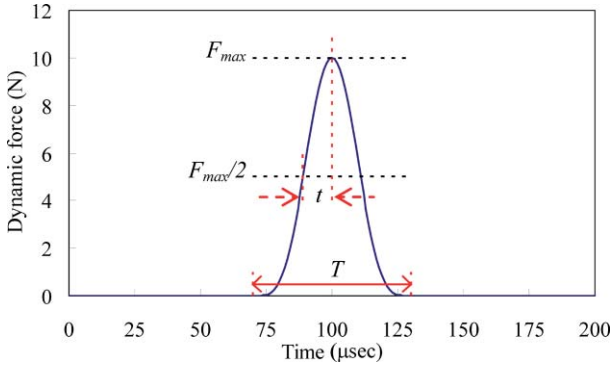

FIG. 5. (Color online) Shape of an *ideal* HNSW.

can be used to induce precompression on a chain of spherical beads, independent from the control of the striker velocity.

The shape of an ideal HNSW is expressed by a function $A\cos^4(\omega t + \varphi)$,[2,17,18] and it is represented as in Fig. 5. The duration T of the pulse can be calculated as

$$T = \frac{2\pi}{\pi - 2\sin^{-1}(2^{-1/4})} t \approx 5.49t, \tag{9}$$

where t is the half width at half maximum amplitude.

In this study the experimental value of t was measured for each time history and the duration T was calculated using Eq. (9). The values of the duration as a function of the dynamic contact force for three values of the precompression force are presented in Fig. 6. The theoretical predictions from Eq. (1) are superimposed to experimental values, for comparison. It is evident that as the temporal pulses' duration decreases, the dynamic force magnitude increases. The experimental data presented in Fig. 6 show that the temporal duration of the solitary waves is nonlinearly dependent on the dynamic contact force.

IV. ACTUATOR 2

Figure 7 shows a photo and the schematic of the second actuator developed in this study. It consisted of a 4.8 mm diameter PTFE tube containing 20 stainless steel beads. Each bead was 4.76 mm in diameter and 0.45 g in mass. A low-carbon steel bead, with the same mass, was used as a striker. The PTFE tube was surmounted by an electromagnet consisting of a coil of a AWG24 magnetic wire wrapped around an iron core. The iron core was a 13 mm diameter and 33 mm long rod. The coil consisted of about 1100 turns and its electric resistance was equal to 7.4 Ω. The electromagnet was collocated inside a second PTFE tube with internal diameter equal to 39 mm, designed to accommodate also the tube containing the chain of particles. Once activated, the electromagnet was able to lift the striker up to a maximum height of 10 mm. For this actuator, the particles used to assemble the chain were made of a nonferromagnetic material to avoid undesired interactions between the beads in the chain and the electromagnet.

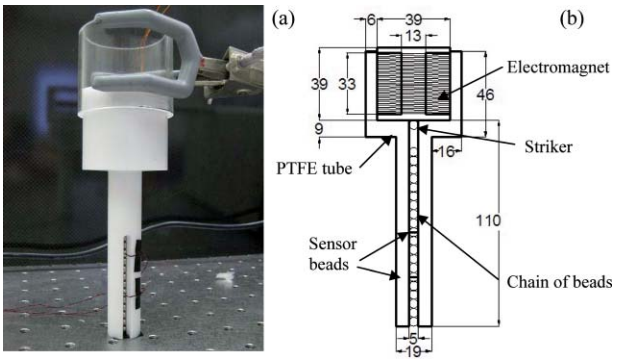

FIG. 7. (Color online) (a) Photo of the designed HNSW actuator. (b) Schematic diagram of the designed HNSW actuator. The units are expressed in mm.

In order to further increase the range of impact velocities achievable with this actuator design, the direct current flowing in the electromagnet can be increased or the design of the coil can be modified by increasing the number of turns per unit length.

We evaluated the capability of the actuator to generate HNSWs positioning two sensor beads at particles number 10 and 15 from the top. For this experiment the falling distance

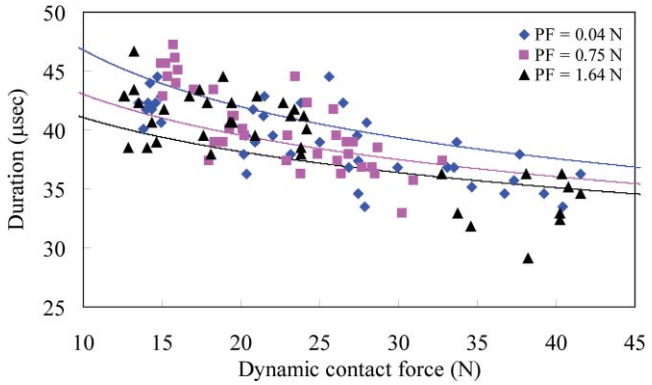

FIG. 6. (Color online) Duration of the traveling pulse as a function of the dynamic contact force at different amounts of static precompression force. The experimental values are shown by solid dots. The theoretical curves based on Eq. (1) for the different values of static precompression applied to the chain are represented by solid lines. (For clarity, the error bars are omitted. The estimated error is ± 5 μs.)

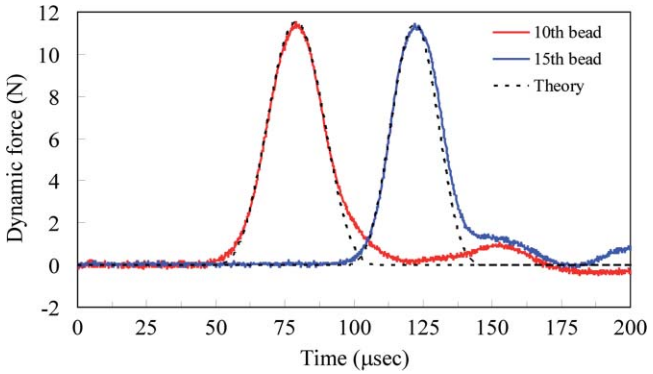

FIG. 8. (Color online) Comparison of the pulse shape obtained using actuator 2 with a theoretical $\cos^4$ function. The first pulse represents the experimental signal recorded by the sensor positioned in the 10th particle from the top of the chain. The second pulse represents the experimental signal recorded by the sensor positioned in the 15th particle from the top of the chain.

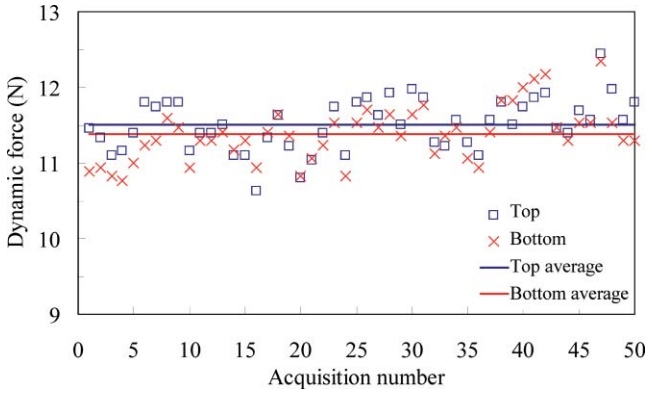

FIG. 9. (Color online) Values of the dynamic force measured by both sensor beads. The horizontal lines represent the mean value recorded by the 10th particle and by the 15th particle.

of the striker was set equal to 8.5 mm. Identical impacts were repeated 50 times to assess the reproducibility and stability of the actuation mechanism. Typical time history of the force measured by both piezosensors is presented in Fig. 8, where the experimental results are superimposed to a $\cos^4$ function. The agreement between the experimental and the ideal pulses is evident.

Figure 9 shows the maximum dynamic force obtained in all 50 measurements extracted from the 10th and 15th beads. The mean value of the dynamic force measured at the 10th particle was equal to 11.51 N with a standard deviation equal to 0.34 N, which is only 2.98% of the mean value. The average value recorded by the 15th particle was equal to 11.38 $\pm$ 0.36 N. In this case, the standard deviation was equal to 3.17% of the mean value. The small standard deviations indicate the high repeatability of the signal generated with this actuator. It should be noted that the average dynamic force measured by the top sensor bead is only 1.17% greater than that measured by the bottom sensor bead. This indicates that the pulse's attenuation in the actuator was very small.

Finally, the speed of the HNSW was calculated detecting the arrival time of the pulse's peak in the instrumented beads and knowing their relative distance in the chain. Figure 10 shows the experimentally calculated wave speed as a function of the dynamic contact force. The theoretical prediction obtained from the long wave approximation is superimposed (red solid line). The agreement between experimental data and theoretical prediction is very good and it confirms the ability of the actuator to generate HNSWs.

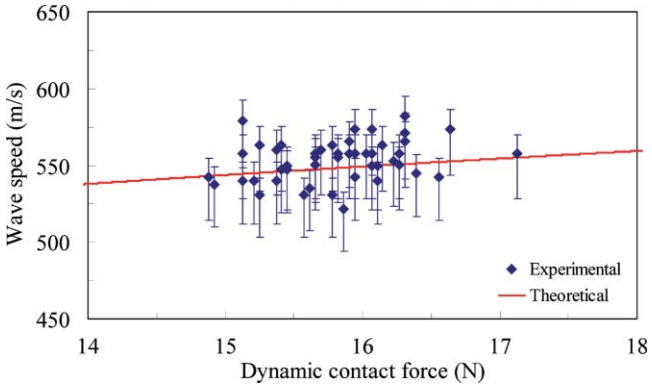

FIG. 10. (Color online) Wave speed as a function of the dynamic contact force at static precompression equal to 0.053 N. The theoretical curve is based on Eq. (1). The vertical error bars are the results of possible inaccuracy on the estimation of the peak's arrival time and on the measurement of the travel distance between the two piezosensors.

V. CONCLUSIONS

This paper presents the design of two actuators for the generation of highly nonlinear solitary waves. Both actuators consist of a small diameter tube containing a chain of particles. This geometry is known to be the simplest arrangement to induce the propagation of highly nonlinear solitary waves. The novelty of the proposed actuators is represented by the presence of an electromagnet that either surrounds or surmounts the chain.

In the first actuator presented, the electromagnet is positioned around the chain to induce static precompression that can be varied at convenience. The electrical current passing through the wire can be adjusted to induce a static force up to 1.64 N. The advantage of the proposed design is the ability to modify the amount of force applied to the chain for tuning certain characteristics of the generated pulses, such as wave speed and amplitude.

In the second actuator presented, an electromagnet was used to strike the chain with particles dropped from controlled heights, function of the current applied to the system. This design allows increasing the repetition rate of the generated pulses which, in turn, can be useful in certain applications such as nondestructive testing. Ongoing research is adopting the second actuator for the nondestructive assessment of concrete structures and concrete hydration process.

ACKNOWLEDGMENTS

This work was supported by the National Science Foundation Grant No. CMMI-0825983 (Dr. Eduardo Misawa, Program Director). C.D. acknowledges support from NSF/CMMI-0844540 (Career). P.R. and X.N. also thank the 2009 ASNT Fellowship Award.

[1] V. F. Nesterenko, J. Appl. Mech. Tech. Phys. **24**, 733 (1984).
[2] V. F. Nesterenko, *Dynamics of Heterogeneous Materials* (Springer-Verlag, New York, 2001), Chap. 1.
[3] C. Coste, E. Falcon, and S. Fauve, Phys. Rev. E **56**, 6104 (1997).
[4] C. Coste and B. Gilles, Eur. Phys. J. B **7**, 155 (1999).
[5] S. Sen, M. Manciu, and J. D. Wright, Phys. Rev. E **57**, 2386 (1998).
[6] M. Manciu, S. Sen, and A. J. Hurd, Physica A **274**, 588 (1999).
[7] M. Manciu, S. Sen, and A. J. Hurd, Physica A **274**, 607 (1999).
[8] J. Hong and A. Xu, Appl. Phys. Lett. **81**, 4868 (2002).
[9] C. Daraio, V. F. Nesterenko, E. B. Herbold, and S. Jin, Phys. Rev. E **72**, 016603 (2005).
[10] C. Daraio and V. F. Nesterenko, Phys. Rev. E **73**, 026612 (2006).
[11] V. F. Nesterenko, C. Daraio, E. B. Herbold, and S. Jin, Phys. Rev. Lett. **95**, 158702 (2005).
[12] C. Daraio, V. F. Nesterenko, E. B. Herbold, and S. Jin, Phys. Rev. Lett. **96**, 058002 (2006).
[13] C. Daraio, V. F. Nesterenko, E. B. Herbold, and S. Jin, Phys. Rev. E **73**, 026610 (2006).
[14] M. A. Porter, C. Daraio, E. B. Herbold, I. Szelengowicz, and P. G. Kevrekidis, Phys. Rev. E **77**, 01560 (2008).
[15] M. A. Porter, C. Daraio, I. Szelengowicz, E. B. Herbold, and P. G. Kevrekidis, Physica D **238**, 666 (2009).

[16]E. B. Herbold, J. Kim, V. F. Nesterenko, S. Wang, and C. Daraio, Acta Mech. **205**, 85 (2009).
[17]D. Khatri, C. Daraio, and P. Rizzo, Proc. SPIE **7292**, 72920P (2009).
[18]J. Hong, J. Y. Ji, and H. Kim, Phys. Rev. Lett. **82**, 3058 (1999).
[19]J. Hong, Phys. Rev. Lett. **94**, 108001 (2005).
[20]S. Job, F. Melo, A. Sokolow, and S. Sen, Phys. Rev. Lett. **94**, 178002 (2005).
[21]L. Vergara, Phys. Rev. Lett. **85**, 108002 (2005).
[22]L. Vergara, Phys. Rev. Lett. **104**, 118001 (2010).
[23]G. Theocharis, M. Kavousanakis, P. G. Kevrekidis, C. Daraio, M. A. Porter, and I. G. Keverekidis, Phys. Rev. E **80**, 066601 (2009).
[24]F. Fraternali, M. A. Porter, and C. Daraio, Mech. Adv. Mater. Struct. **17**, 1 (2010).
[25]R. Carretero-González, D. Khatri, M. A. Porter, P. G. Kevrekidis, and C. Daraio, Phys. Rev. Lett. **102**, 024102 (2009).
[26]X. Ni, R. Garden, and P. Rizzo, in *Proceedings of the 7th International Workshop on Structural Health Monitoring, Palo Alto, 2009*, edited by F. K. Chang (Stanford University, Palo Alto, 2009), p. 996.
[27]X. Ni, P. Rizzo, and C. Daraio, Proc. SPIE **7292**, 729218 (2009).
[28]X. Ni, R. Garden, and P. Rizzo, Proc. SPIE **7647**, 76470S (2010).
[29]A. Spadoni and C. Daraio, Proc. Natl. Acad. Sci. U.S.A. **107**, 7230 (2010).